Quantifying fault connectivity drilling hazards through simple flow computations

Rafael Pires de Lima* and Kurt Marfurt, University of Oklahoma

Summary

Faults can enhance production when confined to the reservoir and impede production when connected to a nearby aquifer, such as those that connect the Eagle Ford Shale to the deeper Edwards Limestone.

These faults constitute geohazards during drilling and a potential water stringer during production, and hence need to be avoided at any cost. Many shale resource plays within the United States lie on or near similar carbonate aquifers such as "Eagle Ford - Edwards", some of which are also karstified.

While faults provide crucial geologic information that can be critical for reservoir modeling, large surveys may contain hundreds of faults requiring significant interpretation effort.

We propose a simple image processing algorithm (in contrast to a more accurate reservoir simulator) with the potential to highlight those faults that may be connected to nearby aquifers. We envision coupling this tool with statistical analysis of water production to identify faults that are safe to complete and those that need to be avoided.

Introduction

The use of edge detecting algorithms on 3D seismic data volumes such as coherence is a valuable tool for highlighting morphological geological features such as channel and faults.

Gersztenkorn and Marfurt (1999) showed that coherence may be evaluated based on cross-correlation between the seismic traces, semblance or with a eigendecomposition of the seismic data covariance matrix. Höcker and Fehmers (2002) and Marfurt (2006) proposed a more robust estimation of dip and azimuth, yielding an increased resolution of coherence computations (as well as other 3-D seismic attributes dip and azimuth dependent).

While faults provide crucial geologic information that can be critical for reservoir modeling, fault picking and interpretation is a time-consuming activity. Nonetheless, there has been little effort for a better fault enhancement and analysis (Machado et al., 2016).

Apart from being a potential conduit for water from underlaying aquifer and drilling geohazard, collapse features and faults often provide conductivity for fluid flow and the presence of these elements may invalidate layers that otherwise could be used for carbon sequestration.

Our objective is to develop a "quick and dirty" image processing algorithm (in contrast to a more accurate reservoir simulator) that will highlight those faults that may be connected to nearby aquifers. Our next objective will be to match the results obtained with this image processing tool with statistical analysis of water production.

Our hypothesis is that faults seen on seismic data will act as conductors between two sets of horizons – or aquifers – that will act as sources or sinks.

Mapping the flow would then be sufficient to highlight the faults that connects both horizons – one source and one sink, while the unconnected faults should have a weaker response. We are aware that faults can be "dip sealing" or "dip leaking" and we understand that the same fault can have different sealing behavior depending on the lithology.

However, the simplistic approximation that coherence attributes are proportional to the hydraulic conductivity may prove itself useful on scenarios where the faults are not completely characterized. In our simulation, we will also assume single phase fluid system and no phase transformation i.e. fluid above bubble point or dew point pressure.

Methodology

We have assumed that the 3D volumetric result of an edge detecting attribute such as coherence is representative of thermal, electrical or hydraulic conductivity. Hence, we can use these attributes as a proxy of conductivity to simulate the steady-state flow between two horizons.

The two horizons on this conductivity scheme are: the aquifer layer (to be modeled as the source) and the reservoir layer (to be a sink).

We will first calculate the fluid head (h) using the three-dimensional steady-state saturated flow equation (Istok, 2013; Harbaugh, 2005):

$$\frac{\partial}{\partial x}\left(K_x \frac{\partial h}{\partial x}\right) + \frac{\partial}{\partial y}\left(K_y \frac{\partial h}{\partial y}\right) + \frac{\partial}{\partial z}\left(K_z \frac{\partial h}{\partial z}\right) = 0, \quad (1)$$

where K_x, K_y, and K_z are the conductivities of the media in the x, y and z coordinate directions. This equation is commonly used for groundwater flow modeling. Next, we will calculate the absolute flow **q** using:

$$\mathbf{q} = q_x\hat{\boldsymbol{x}} + q_y\hat{\boldsymbol{y}} + q_z\hat{\boldsymbol{z}} = -K_x\frac{\partial h}{\partial x}\hat{\boldsymbol{x}} - K_y\frac{\partial h}{\partial y}\hat{\boldsymbol{y}} - K_x\frac{\partial h}{\partial z}\hat{\boldsymbol{z}}, (2)$$

SEG International Exposition and 87th Annual Meeting

where $\hat{\boldsymbol{x}}$, $\hat{\boldsymbol{y}}$ and $\hat{\boldsymbol{z}}$ are the unit vectors for x, y and z directions respectively. We expect to observe the conductors connecting source and sink with a higher absolute flow value, $|\mathbf{q}|$, compared to the other areas.
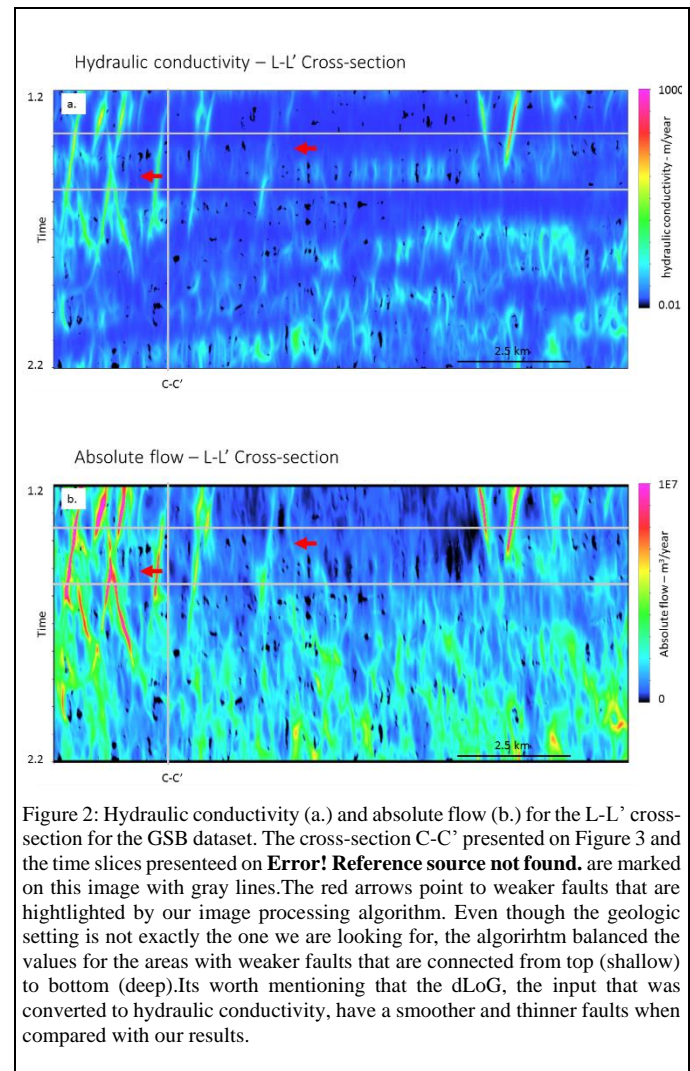
Results

Figure 1 shows the results obtained using a simple synthetic model with vertical faults along with the intermediate step

Figure 1: Cross-section of a 3D synthetic model with connected and not connected faults. The background hydraulic conductivity (panel a.) is 10 m/year while the stronger pink faults have a value of 1000 m/year. Also on panel a., the weaker blue fault has a hydraulic conductivity of 100 m/year. The potential head results is displayed on panel b. while the final absolute flow is displayed on panel c. On all panels, the red arrows point to connected faults, the gray arrow point to the not connected fault. The gray circle highlights the break point of a fault that is not connected due to our finite difference scheme. Even the rightmost fault, with a smaller hydraulic conductivity, is highlighted with the algorithm.

of the algorithm, the calculation of the potential field. The connected faults, those that link the potential reservoir with the overpressured aquifer below, have a higher anomalous value for the absolute flow as expected. The gray arrow and the gray circle show that the disjoint faults have weaker absolute flow.

Figure 2**,** Figure 3 and **Error! Reference source not found.** show results obtained testing our algorithm with real seismic data as input. The hydraulic conductivity is a scaled value of the result obtained with the directional Laplacian of a Gaussian (dLoG) attribute described by Machado et al. (2016). The dLoG operator sharpen fault features within a coherence seismic attribute volume (Machado et al., 2016). The seismic data was acquired is from a survey over the

Figure 2: Hydraulic conductivity (a.) and absolute flow (b.) for the L-L' cross-section for the GSB dataset. The cross-section C-C' presented on Figure 3 and the time slices presenteed on **Error! Reference source not found.** are marked on this image with gray lines.The red arrows point to weaker faults that are hightlighted by our image processing algorithm. Even though the geologic setting is not exactly the one we are looking for, the algorirhtm balanced the values for the areas with weaker faults that are connected from top (shallow) to bottom (deep).Its worth mentioning that the dLoG, the input that was converted to hydraulic conductivity, have a smoother and thinner faults when compared with our results.

Quantifying fault connectivity drilling hazards through simple flow computations

Great South Basin (GSB), off the southeast coast of South Island of New Zealand. The dLoG values were scaled so they would vary from 0.01 to 1000 m/year.

To have a better geological significance, the top and bottom limits for the potential calculations should be based on geological horizons. However, for the initial testing, we limited the computations solely based on time slices. The GSB does not have the geological setting we were looking for when we designed and prototyped the algorithm, a potential unconventional reservoir sitting atop of a overpressured aquifer. Nonetheless, interesting results can be observed.

Computing the absolute flow on the GSB balanced the value of smaller and weaker faults, highlighting geological features that may otherwise be overlooked. The geometrical behavior of faulting displayed on **Error! Reference source not found.** that perhaps may be an indicative of presence of syneresis became clearer on the absolute flow results.

Conclusions and Future Work

We have prototyped a very simple flow model that is built on the hypothesis that seismic attributes such as coherence delineate conductive faults. While such a simple flow model cannot replace more carefully (and interpreter intensive!) models built in commercial flow simulators, it can be used to statistically correlate water production from a suite of horizontal wells to azimuthally limited fault families.

Such correlations may help us avoid problematic faults or target those that may enhance production. We envision that applying the procedure described on this abstract can be used for predicting faults that can have a higher water inflow from a deeper aquifer.

On a different geological background, such as the one on the GSB dataset, the absolute flow computation was useful to better visualize geometrical geological features that maybe overlooked. Small faults that might seem unimportant or discontinuous could be indicators of a more complex geological environment.
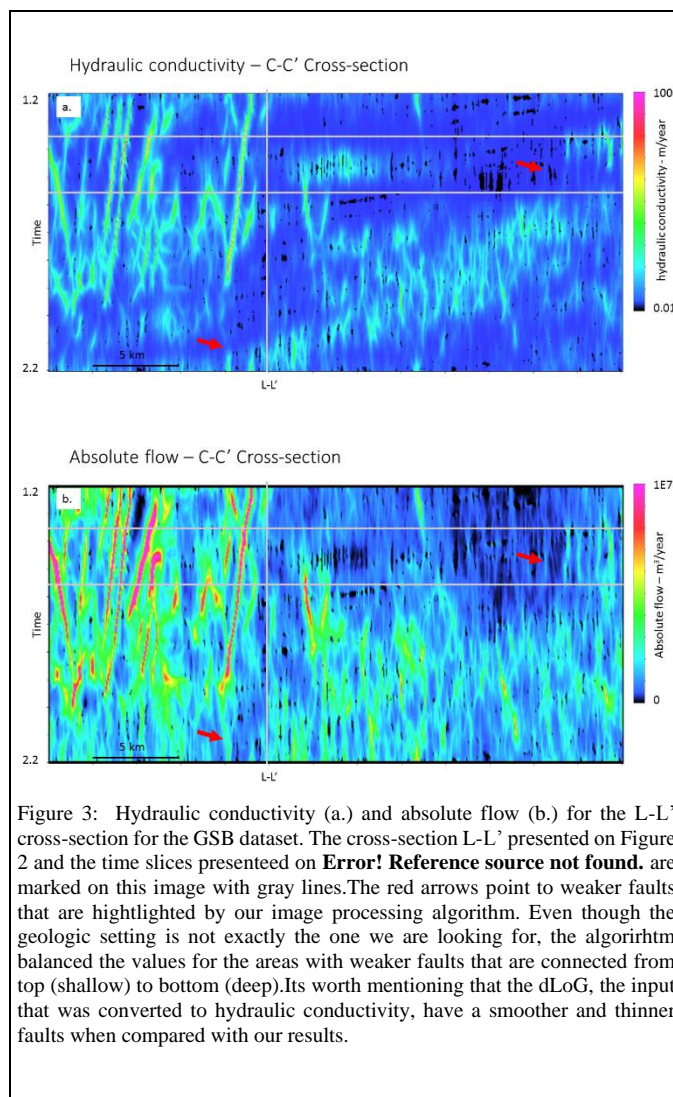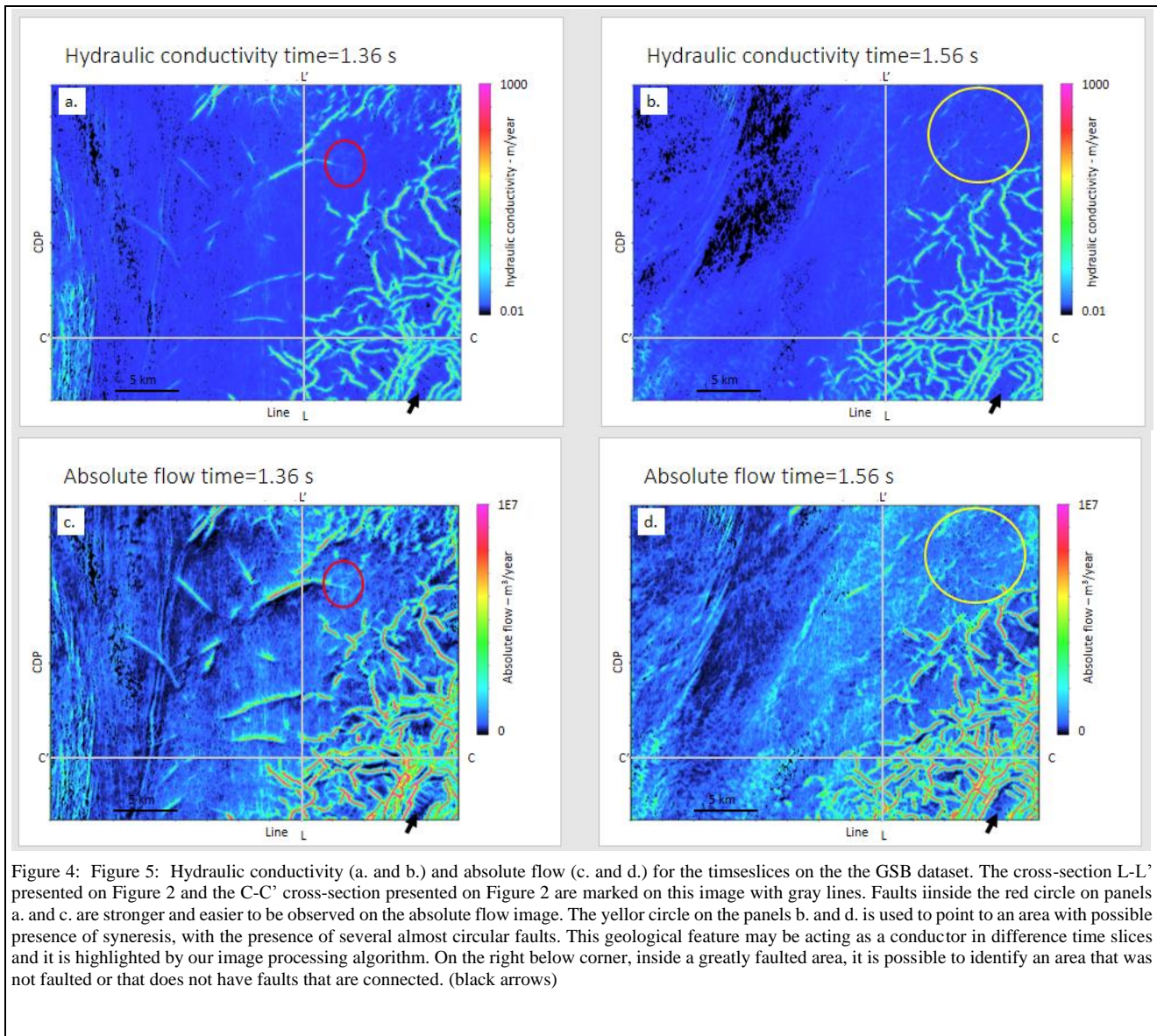
Acknowledgements

Figure 3: Hydraulic conductivity (a.) and absolute flow (b.) for the L-L' cross-section for the GSB dataset. The cross-section L-L' presented on Figure 2 and the time slices presenteed on **Error! Reference source not found.** are marked on this image with gray lines.The red arrows point to weaker faults that are hightlighted by our image processing algorithm. Even though the geologic setting is not exactly the one we are looking for, the algorirhtm balanced the values for the areas with weaker faults that are connected from top (shallow) to bottom (deep).Its worth mentioning that the dLoG, the input that was converted to hydraulic conductivity, have a smoother and thinner faults when compared with our results.

Quantifying fault connectivity drilling hazards through simple flow computations

Figure 4: Figure 5: Hydraulic conductivity (a. and b.) and absolute flow (c. and d.) for the timseslices on the the GSB dataset. The cross-section L-L' presented on Figure 2 and the C-C' cross-section presented on Figure 2 are marked on this image with gray lines. Faults iinside the red circle on panels a. and c. are stronger and easier to be observed on the absolute flow image. The yellor circle on the panels b. and d. is used to point to an area with possible presence of syneresis, with the presence of several almost circular faults. This geological feature may be acting as a conductor in difference time slices and it is highlighted by our image processing algorithm. On the right below corner, inside a greatly faulted area, it is possible to identify an area that was not faulted or that does not have faults that are connected. (black arrows)

EDITED REFERENCES

Note: This reference list is a copyedited version of the reference list submitted by the author. Reference lists for the 2017 SEG Technical Program Expanded Abstracts have been copyedited so that references provided with the online metadata for each paper will achieve a high degree of linking to cited sources that appear on the Web.

REFERENCES

Gersztenkorn, A., and K. J. Marfurt, 1999, Eigenstructure-based coherence computations as an aid to 3-D structural and stratigraphic mapping: Geophysics, **64**, 1468–1479, http://dx.doi.org/10.1190/1.1444651.

Harbaugh, A. W., 2005, Chapter 2 – Derivation of the finite-difference equation, MODFLOW-2005. U.S. Geological Survey, 2.1–2.17.

Höcker, C., and G. Fehmers, 2002, Fast structural interpretation with structure-oriented filtering: The Leading Edge, **21**, 238–243, http://dx.doi.org/10.1190/1.1463775.

Istok, J., 2013, Step 2: Derive the approximating equations, groundwater modeling by the finite element method: American Geophysical Union, 30–79.

Machado, G., A. Alali, B. Hutchinson, O. Olorunsola, and K. J. Marfurt, 2016, Display and enhancement of volumetric fault images: Interpretation, **4**, SB51–SB61, http://dx.doi.org/10.1190/INT-2015-0104.

Marfurt, K. J., 2006, Robust estimates of 3D reflector dip and azimuth: Geophysics, **71**, no. 4, P29–P40, http://dx.doi.org/10.1190/1.2213049.